01 Sep 2006

Flow Regime Identification in a Bubble Column based on Both Statistical and Chaotic Parameters Applied to Computed Tomography Data

Stoyan Nedeltchev

Ashfaq Shaikh

Muthanna H. Al-Dahhan
Missouri University of Science and Technology, aldahhanm@mst.edu

Recommended Citation

S. Nedeltchev et al., "Flow Regime Identification in a Bubble Column based on Both Statistical and Chaotic Parameters Applied to Computed Tomography Data," *Chemical Engineering and Technology*, vol. 29, no. 9, pp. 1054 - 1060, Wiley; Gesellschaft Deutscher Chemiker; Gesellschaft für Chemische Technik und Biotechnologie, Sep 2006.
The definitive version is available at https://doi.org/10.1002/ceat.200600162

Stoyan Nedeltchev[1]
Ashfaq Shaikh[2]
Muthanna Al-Dahhan[2]

[1] Institute of Technical Chemistry, TU Braunschweig, Germany.

[2] Department of Chemical Engineering, Washington University in St. Louis, Chemical Reaction Engineering Laboratory, MO, USA.

Full Paper

Flow Regime Identification in a Bubble Column Based on Both Statistical and Chaotic Parameters Applied to Computed Tomography Data

The Kolmogorov entropy (KE) algorithm was applied successfully to single source γ-ray Computed Tomography (CT) data measured in a 0.162 m ID bubble column equipped with a perforated plate distributor (163 holes $\cdot \varnothing$ 1.32 mm). Dried air was used as the gas phase and Therminol LT (ρ_L = 886 kg m^{-3}, μ_L = $0.88 \cdot 10^{-3}$ Pa s, σ = $17 \cdot 10^{-3}$ N m^{-1}) was used as a liquid phase. Three different pressures, P, of 0.1, 0.4, and 1.0 MPa were examined. At each pressure the superficial gas velocity, u_G, was increased stepwise by steps of 0.01 m s^{-1} up to 0.2 m s^{-1}. The average absolute deviation (AAD) was also used as a robust statistical criterion for regime transition. At all three pressures, based on the sudden changes in both the AAD and KE values, the boundaries of the following five regimes were identified: dispersed bubble regime, first and second transition regimes, coalesced bubble regime consisting of four regions (called 4-region flow), and coalesced bubble regime consisting of three regions (called 3-region flow). The existence of these regimes has already been documented. As the pressure increases, the transition velocity between the dispersed bubble and first transition regimes and the transition velocity between coalesced bubble (4-region flow) and coalesced bubble (3-region flow) regimes shift to higher u_G values. On the other hand, at P = 0.4 MPa the second transition regime starts earlier. In addition, at P = 1 MPa the transition to coalesced bubble (4-region flow) is delayed.

Keywords: Bubble columns, Chaotic behavior, Computed tomography data, High pressure

Received: May 26, 2006; *accepted:* June 24, 2006

DOI: 10.1002/ceat.200600162

1 Introduction

Bubble columns (BCs) are finding increasing application in chemical, petroleum, biochemical and environmental processes due to their simple construction, ease of temperature control and good heat and mass transfer characteristics. The BC performance can change significantly as a result of flow regime change [1]. Since reactor volume productivity, mass transfer, heat transfer, and mixing are affected by the prevailing flow regime, it is very important to know how to identify it. A good knowledge of the BC hydrodynamics and flow regime transitions is required for design, operation, control and scale-up purposes. The demarcation criteria of the flow regimes may vary with design or operating variables such as column diameter, type of gas distributor, gas density, and liquid properties [2].

1.1 Description of Flow Regimes

Three major flow regimes are commonly encountered in BCs: dispersed bubble (homogeneous), transition, and coalesced bubble (heterogeneous). The dispersed bubble regime is characterized by gentle agitation of the gas-liquid dispersion by relatively small uniform bubbles. The bubble size distribution is very narrow and it is only influenced by the gas sparger. The bubble streams are observed to rise rectilinearly. Bubble coalescence is insignificant. Dynamic vortices may be observed occasionally as the bubbles rise. A relatively uniform gas holdup profile and a rather flat liquid velocity profile are observed.

Correspondence: Dr. S. Nedeltchev (snn13@gmx.net), Institute of Technical Chemistry, TU Braunschweig, Hans-Sommer-Strasse 10, D-38106 Braunschweig, Germany.

The transition regime is characterized by large flow macrostructures (large eddies) and widened bubble size distribution due to the onset of bubble coalescence. This regime corresponds to the development of local liquid circulation patterns in the column. It is well established that the occurrence and the persistence of the transition regime depends largely on the uniformity and the quality of the aeration. Recently Olmos et al. [3, 4] and Barghi et al. [5] provided evidence of the existence of both first and second transition regimes. In the first transition regime, the large bubbles are formed only in the distributor region, whereas in the second transition regime the bulk region coalescence and breakup, together with the development of gross liquid circulation effects begin to dominate. Olmos et al. [3] argue that the flow structure is not well established in the first transition regime. Bubble coalescence only occurs near the sparger. The individual bubble plumes are transformed into an oscillating plume of gathered bubbles. However, this central plume is unstable and beyond a certain liquid height, the flow structure returns to that existing in the dispersed bubble regime with individual trajectories. As the superficial gas velocity, u_G, increases, this critical liquid height reaches the liquid dispersion height and the fully established second transition regime is reached [3]. In this transition regime, a global liquid flow macrostructure appears.

Olmos et al. [4] argue that in the first transition regime, the established flow pattern is still homogeneous despite some predominating bubble paths in the column center. Near the gas distributor, the flow structures evolve and liquid macrostructures occur. Many bubbles occupy the core region. In the second transition regime the occurrence of the large liquid flow macrostructures and the concentration of the bubbles in the column center become more pronounced. The distributor effects become less important [4].

As u_G increases, larger bubbles start to form whose wakes cause gross circulation patterns in the bubble bed leading to coalesced bubble (churn-turbulent) regime. The transition from dispersed bubble to coalesced bubble regime is a gradual process. The coalesced bubble regime is characterized by the wide distribution of bubble sizes and by the existence of a radial gas holdup profile which causes liquid circulation. In this regime, coalescence and breakup occur. Bubbles agglomerate in the vicinity of the gas distributor to form larger bubbles. The coalesced bubble regime is characterized by vigorous mixing. It is argued that in this regime the gas distributor has little effect [6].

Additionally, Fan and coworkers [2, 7] reported the existence of a coalesced bubble regime consisting of four regions (called 4-region flow) and a coalesced bubble regime consisting of three regions (called 3-region flow). The four regions were named as follows: central fast bubble, central plume, vortical and descending regions. In the case of a coalesced bubble (3-region flow) regime, the central plume region becomes indistinguishable from the central fast bubble region (formed by the coalesced large bubbles).

In the coalesced bubble (4-region flow) regime there is a spiral, but chaotic liquid flow pattern. It is characterized by a gross liquid circulation, wherein the liquid rises in the middle portion of the column and descends adjacent to the sidewalls. The liquid flow pattern is much more chaotic and dynamic than that in both transition regimes [2]. The liquid mixing between the bottom and the top of the column is not as rapid as that in the transition regimes.

In the central fast bubble flow region, significant bubble coalescence and breakup occur. The liquid flow is dominated by the wake effects from the large bubbles rising in the central part of the column. In this region, bubble clusters or coalesced bubbles move upward in a spiral manner with high velocity. The central fast bubble flow region is not only rotating, but also rising up axially. The central plume region is located in the column core and is surrounded by the fast bubble flow region. It is characterized by a relatively uniform bubble size distribution, and less bubble-bubble interaction (coalescence). As u_G increases, the fast bubble flow region grows inward, swinging in a wavelike manner, while the central plume region progressively diminishes. The descending flow region, located adjacent to the column wall, is characterized by downward liquid streams moving in either a straight or spiral manner depending on u_G. The size of this region changes with u_G [2]. The vortical region consists of multiple vortices located along the column walls in the axial direction. The entire vortical region is swinging laterally back and forth, in a manner closely related to the swinging motion of the neighboring fast bubble region. The migration of the bubbles away from the sidewalls causes bubble coalescence and the creation of the fast bubble flow region which strengthens both the vortical and descending regions [7]. Local chaotic motion of the liquid phase, caused by the bubble wake and drift effects due to the bubble motion, progressively destroys the vortical and spiral flow structure and leads to the turbulent flow structure. Both coalesced bubble subregimes are characterized with coherent structures. Nedeltchev et al. [8, 9] identified the boundaries of the aforementioned five regimes by means of a nonlinear chaos analysis applied to both liquid concentration and gas holdup fluctuations.

1.2 Application of Chaos Analysis to Bubble Columns

Numerous studies have been devoted to flow regime identification in gas-liquid BCs [6, 10]. The regime transition identification was based on Computed Tomography (CT) data [10], conductivity probe signals [11–15], etc. Chaos analysis in the field of BCs was applied to mass transfer data [8], gas holdup fluctuations [9], pressure fluctuations [16–20], bubbling frequency [21], and Computer-Automated Radioactive Particle Tracking (CARPT) data [22, 23]. All of the aforementioned studies have demonstrated that the nonlinear chaos analysis can provide important insights into the complex hydrodynamics of BCs. Nonlinear chaos analysis can be used for a quantitative characterization of various regime transitions in a BC.

The BC can be regarded as a chaotic system, that is, as a system governed by nonlinear interactions between the system variables. Due to the nonlinearity, this deterministic system is sensitive to small changes in initial conditions and is, therefore, characterized by a limited predictability. The dynamics of the chaotic system are fully represented by the so-called

strange attractor in the phase space. The attractor of the chaotic system is not finite and the system never returns to the same state. The most important concept to analyze chaos from a complex time series is to unfold the hidden chaotic attractor [17]. Van den Bleek and Schouten [24] developed a reliable technique for attractor reconstruction. These authors have recently published a good review paper on the application of chaos analysis to multiphase reactors [25].

The chaotic system is a nonlinear, deterministic system [26]. A typical feature of the nonlinear system is that it spontaneously develops time-dependent behavior. The chaotic system differs considerably from the system usually encountered, especially with respect to its predictability. The Kolmogorov entropy (KE) quantifies the degree of unpredictability of the system. The KE value reflects the rate of information loss of the system, and thus accounts for the accuracy of the initial conditions that is required to predict the evolution of the system over a given time interval [24]. KE > 0 is a sufficient condition for chaos, and to some extent the chaotic system is only predictable over a restricted time interval. KE is large for very irregular dynamic behavior, small in the case of more regular, periodic like behavior, and zero for completely periodic systems. This parameter is sensitive to changes in operating conditions and as such, can be employed for flow regime identification.

The BC complex behavior can be described by means of the nonlinear chaos theory. The study of chaos has provided new conceptual and theoretical tools enabling a better understanding of this complex behavior. The chaos theory allows the order and universality that underlies these complexities to be observed. For a nonlinear system such as a BC, a small change in a parameter can lead to sudden and dramatic changes in both the qualitative and quantitative behavior of the system. For one value, the behavior might be periodic, whereas for another value only slightly different from the first, the behavior might be completely aperiodic (it never exactly repeats). Some sudden and dramatic changes in the nonlinear system may give rise to the complex behavior called chaos. The time behavior of the BC is described as chaotic when that behavior is aperiodic and is apparently random.

Hence, the focus of this paper is to demonstrate that the nonlinear chaos analysis (the KE concept) can be applied successfully to CT data obtained in a BC for the sake of identification of the boundaries of various flow regimes. To the best of the current authors' knowledge, the nonlinear chaos analysis is applied for the first time to nonintrusive CT data. By means of the chaos theory, attempts to extract information hidden in the CT signals will be presented. The transition velocities determined by means of the KE values will be compared with those identified by a robust statistical (average absolute deviation) parameter.

2 Experimental

The CT experiments were carried out in a 0.162 m ID stainless steel column with a total height of 2.5 m. The column was equipped with a perforated plate distributor (163 holes · ∅ 1.32 mm, 1.09 % open area). A schematic of the experimental setup is presented in Fig. 1. The column is designed to support a maximum operating pressure of 2 MPa.

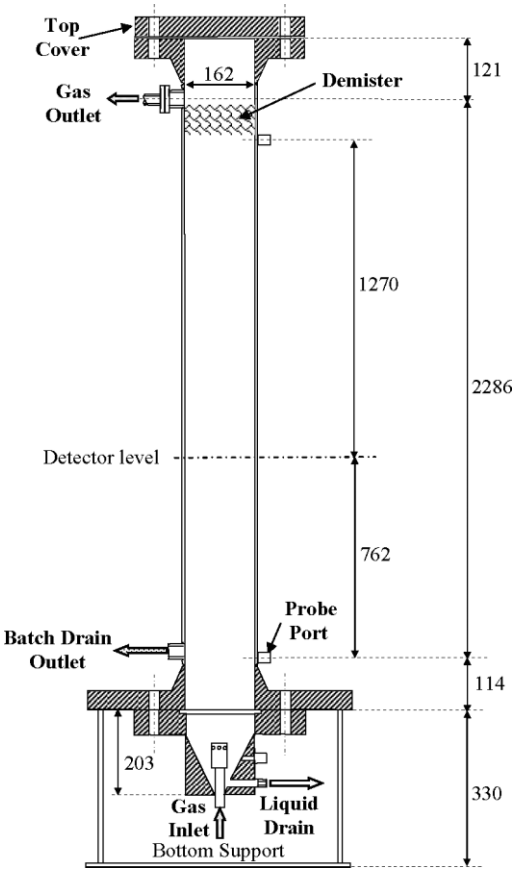

Figure 1. High-pressure stainless steel bubble column (all scales are given in mm).

Air was used as the gas phase. It was supplied from two compressors connected in parallel, with a working pressure of 1.45 MPa and a maximum flow rate of 0.147 $m^3 s^{-1}$. The compressed atmospheric air was dried and purified by passing it through a dryer and several air filter units. The air flow rate was controlled by a pressure regulator and rotameter setup, which consisted of four rotameters of increasing range, connected in parallel.

Air exited the column through a demister, passed through a back pressure regulator that controlled column operating pressure, and was vented to the atmosphere. The column design enables easy removal of the distributor chamber and replacement of the sparger. Further details can be found elsewhere [27, 28].

Therminol LT ($\mu_L = 0.88 \cdot 10^{-3}$ Pa s, $\rho_L = 886$ kg m^{-3}, $\sigma = 17$ N m^{-1}) was used as the liquid phase. The u_G values were varied from 0.01–0.2 m s^{-1} at intervals of 0.01 m s^{-1}. The CT experiments were performed at operating pressures of 0.1, 0.4, and 1 MPa.

2.1 Single Source γ-Ray Computed Tomography (CT)

CT has been extensively implemented on various multiphase flow systems at the Chemical Reaction Engineering Laboratory (CREL), Washington University, to measure cross-sectional

phase holdup distribution. The phase holdup radial profiles can be obtained by azimuthal averaging of cross-sectional values. The radial averaging of the phase holdup profiles can then be used to calculate cross-sectional averaged phase holdups. Software and hardware details of the single source γ-ray CT have been explained elsewhere [29]. The CT setup (see Fig. 2) consists of an array of detectors with an opposing source, which rotate together around the object to be scanned.

The scanner uses a Cesium (Cs-137) encapsulated γ-ray source with activity of ~85 mCi. The array of detectors and the source are mounted on a gantry which can be rotated 360° around the object to be scanned, using a stepper motor interfaced to a host computer. In addition, the source-detector setup can be moved up and down to scan cross-sections at any axial position of the column. In the present study, five NaI scintillation detectors were used which cover the entire cross-section of the 0.162 m ID column. Each detector consists of a cylindrical $0.051 \cdot 0.051$ m NaI crystal, a photo multiplicator and electronics, forming a $0.054 \cdot 0.26$ m cylindrical assembly. In each view, every detector acquires 7 projections covering a total angular span of 2.72° of the detector face. A total of 99 views were acquired, with 3.6° of angular shift after every view. Hence, 3465 projections (from $5 \cdot 7 \cdot 99$) were used to reconstruct the phase holdup distribution at each cross-sectional plane. The entire system is completely automated to acquire the photon count data needed for the reconstruction of the phase holdup distribution in a given cross-section. The estimation-maximization algorithm has been used for image reconstruction [29]. It is based on maximum-likelihood principles and takes into account the stochastic nature of the γ-ray beam projection measurements. Further information about the CT facility can be found elsewhere [10, 30, 31]. As gas holdup radial profiles in the fully developed region are axially invariant [32], all CT scans were performed at $L\,D_c^{-1} = 5.5$. In the current work, statistical and chaotic analysis is applied on the time-series of counts that consist of 10 000 data points obtained by only one detector. These data points consist of counts received at different views as well as projections.

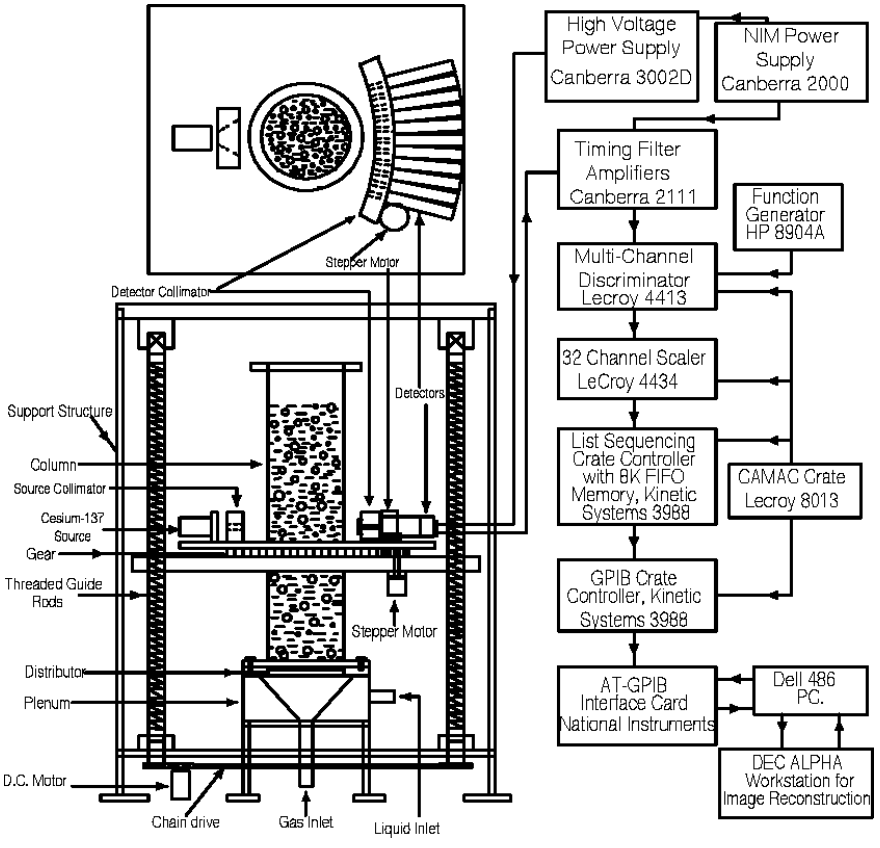

Figure 2. Configuration of the CT experimental setup [29].

3 Results and Discussion

The present paper focuses on the identification of various flow regimes in a BC operated under three different pressures. In general, the pressure effect on the flow regime transition is a result of the variation in bubble characteristics (bubble size and velocity and their distribution). Under high-pressure conditions, bubble coalescence is suppressed and bubble breakup is enhanced. As a result, small bubble sizes and narrow bubble size distributions are observed. These effects delay the flow regime transition in high-pressure BCs and slurry BCs [33]. The flow regime identification is an important first step in the study of BC hydrodynamics.

Fig. 3a) shows the average absolute deviation (AAD) values of the time-averaged cross-sectional distribution of the gas holdup obtained by CT at ambient pressure, as a function of u_G. AAD is a robust statistical estimator of the data width around the mean. This parameter is calculated as follows:

$$\mathrm{AAD} = \left(\sum_{i=1}^{N} |x_i - x_{\mathrm{mean}}|\right)/N \qquad (1)$$

where x_{mean} is the mean of the x_i time series, and N is the number of data in a time series. x_i is the gas holdup in the pixel of the CT cross-section.

It is worth pointing out that the AAD was used as a maximum inter-point distance (cut-off length) in the KE calculations. Based on the sudden changes in the AAD profile it was possible to identify the boundaries of the following five regimes: dispersed bubble ($u_G < 0.02\ \mathrm{m\,s^{-1}}$), first transition ($0.02 \le u_G < 0.08\ \mathrm{m\,s^{-1}}$), second transition ($0.08 \le u_G < 0.1\ \mathrm{m\,s^{-1}}$), coalesced bubble (4-region flow) ($0.1 \le u_G < 0.13\ \mathrm{m\,s^{-1}}$), and coalesced bubble (3-region flow) ($u_G \ge 0.13\ \mathrm{m\ s^{-1}}$).

Fig. 3b) shows the KE values calculated from the time-averaged cross-sectional distribution of the gas holdup obtained by CT at ambient pressure as

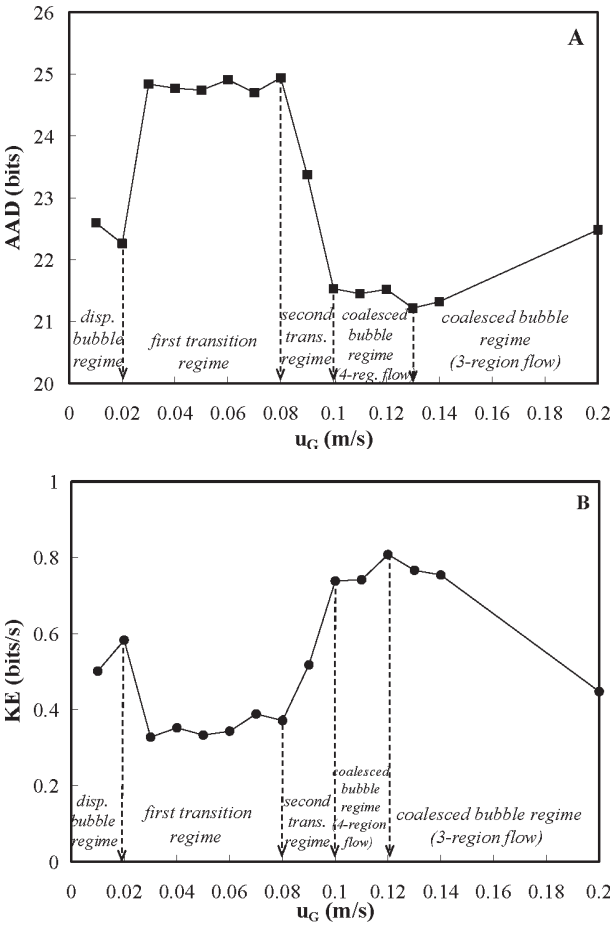

Figure 3. AAD (A) and KE (B) values estimated from CT data obtained at $LD_c^{-1} = 5.5$ as a function of superficial gas velocity u_G, $P = 0.1$ MPa.

a function of u_G. It is worth noting that the sudden changes in the KE values correspond well to the sudden changes in the AAD values. This good match means that the four different regime transition velocities, U_{trans}, determined, should be regarded as reliable. The methods for calculation of the AAD and KE are completely independent. The nonintrusive CT data were treated for the first time by means of the KE algorithm developed by Schouten et al. [34]. The maximum-likelihood estimation method for the KE is based on the exponential divergence of nearby trajectories of the attractor. This property is a signature of chaotic behavior. Following [16] and [23], the embedding dimension was set to 50. It was confirmed that with this embedding dimension the attractors are unfolded in the state space. The state vectors in the reconstructed phase space were formed by using time delay of unity.

Based on the sudden changes (mostly maxima) in the KE values the same boundaries of the aforementioned regimes were identified. Only the coalesced bubble regime (3-region flow) started somewhat earlier at $u_G = 0.12$ m s^{-1}. It is worth noting that in the fully developed coalesced bubble regime (3-region flow) KE starts to decrease monotonously. This implies that the gas-liquid dispersion becomes less chaotic. The same KE behavior was observed when chaos analysis was applied to pressure fluctuations [35]. Lin et al. [17] reported similar behavior of the metric entropy in the fully developed churn-turbulent regime. At each regime transition velocity, U_{trans}, strong and complex disturbances occur since the flow structure changes. Therefore, the KE profile exhibits a local maximum in most cases. The value of the first transition velocity (0.02 m s^{-1}) is close to the value (0.024 m s^{-1}) predicted by the formulas of Reilly et al. [36]. In addition, the criterion reported by Miller [37] predicts that the first transition occurs at 0.021 m s^{-1} ($Re_{0L} = 2000$), whereas the coalesced bubble regime starts at 0.104 m s^{-1} ($Re_{0L} = 10\,000$). These transitional u_G values agree well with the present findings. Nedeltchev and coworkers [8, 9] also reported that the first transition velocity occurs at about 0.02 m s^{-1}. It is worth noting that they used a different liquid and different type of gas distributor. The BC diameter was also smaller. All these facts should be regarded as evidence for the validation of the current AAD and KE calculations based on nonintrusive CT data. Such results are presented for the first time.

Fig. 4a) shows the AAD values at $P = 0.4$ MPa. It is obvious that this robust statistical parameter is again capable of identify-

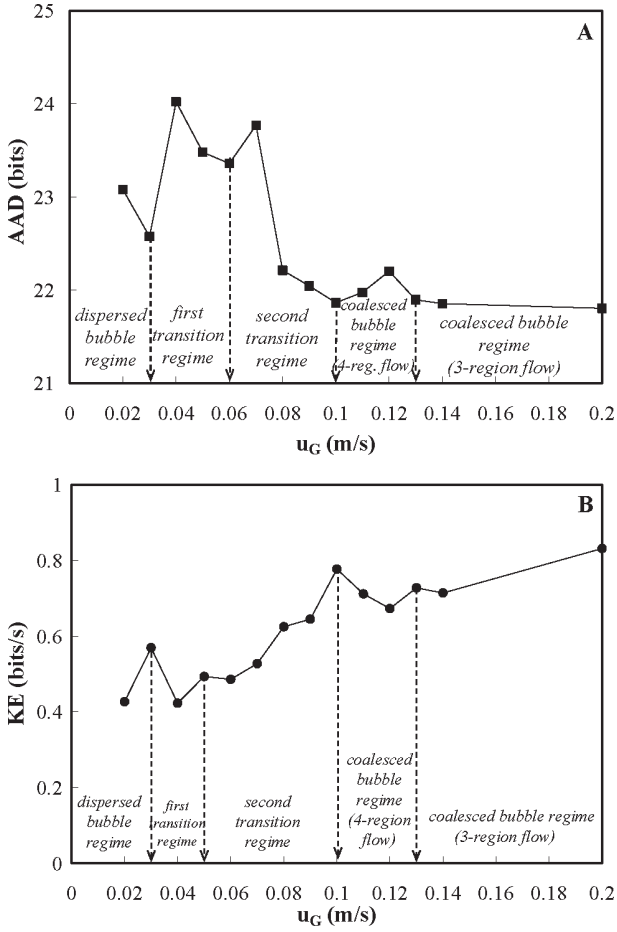

Figure 4. AAD (A) and KE (B) values estimated from CT data obtained at $LD_c^{-1} = 5.5$ as a function of superficial gas velocity u_G, $P = 0.4$ MPa.

ing dispersed bubble ($u_G < 0.03$ m s^{-1}), first transition ($0.03 \le u_G < 0.06$ m s^{-1}), second transition ($0.06 \le u_G < 0.1$ m s^{-1}), coalesced bubble (4-region flow) ($0.1 \le u_G < 0.13$ m s^{-1}), and coalesced bubble (3-region flow) ($u_G \ge 0.13$ m s^{-1}) regimes. At P = 0.4 MPa, the first transition velocity, U_{trans}, shifts to a higher u_G value. In addition, one can note that the second transition regime starts earlier and it spans over a broader u_G range.

Fig. 4b) indicates that the KE maxima correspond well to the AAD minima. Therefore, the boundaries of the flow regimes more or less coincide. The KE maxima at u_G = 0.05 and 0.13 m s^{-1} are not well pronounced, possibly because the differences in the flow structure between the first and second transition regimes and coalesced bubble (4-region flow) and coalesced bubble (3-region flow) regimes are not that large. The only difference between the AAD and KE results, occurs at the transition velocity ,U_{trans}, between first and second transition regimes. The KE results reveal that the second transition regime starts at 0.05 m s^{-1}, whereas the AAD values show that it occurs at 0.06 m s^{-1}. Again, the first U_{trans} value obtained is 0.03 m s^{-1}, while the value predicted by the formulas of Reilly et al. [36] is 0.038 m s^{-1}.

Fig. 5a) shows the AAD values at P = 1 MPa as a function of u_G. Based on the local well pronounced AAD minima the following regimes can be identified: dispersed bubble ($u_G < 0.04$ m s^{-1}), first transition ($0.04 \le u_G < 0.08$ m s^{-1}), second transition ($0.08 \le u_G < 0.13$ m s^{-1}), coalesced bubble (4-region flow) ($0.13 \le u_G < 0.16$ m s^{-1}), and coalesced bubble (3-region flow) ($u_G \ge 0.16$ m s^{-1}). At this pressure, both the first and last transition velocities shift to higher u_G values. The onset of the coalesced bubble (4-region flow) regime is also delayed.

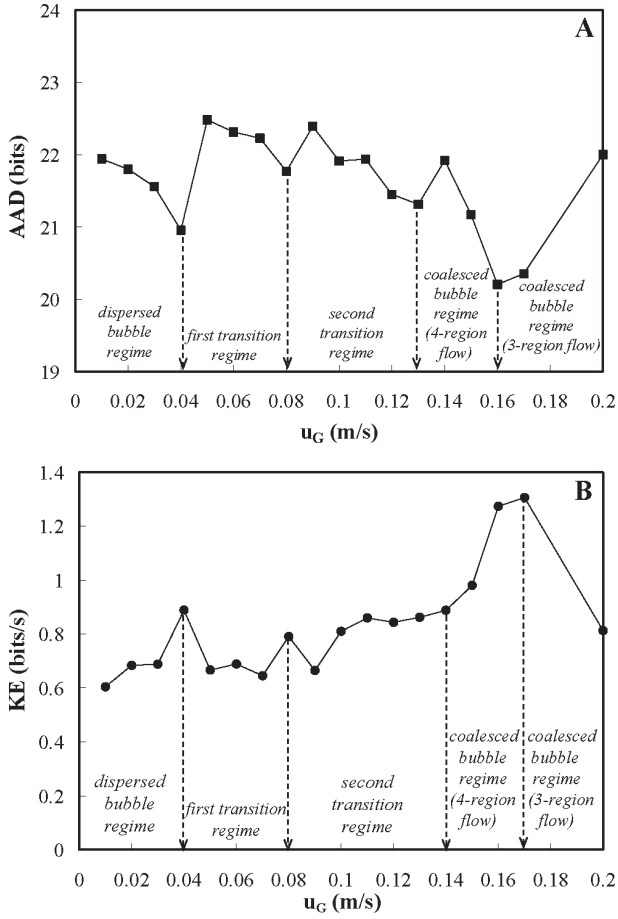

Figure 5. AAD (A) and KE (B) values estimated from CT data obtained at LD_c^{-1} = 5.5 as a function of superficial gas velocity u_G, P = 1.0 MPa.

Fig. 5b) reveals that the KE maxima correspond well to the AAD minima. At u_G = 0.14 m s^{-1} there is no local KE peak but the KE values suddenly start to increase. Fig. 5a) shows that the third regime transition point occurs around this u_G value. Basically, only the last two U_{trans} values are somewhat shifted to higher u_G values. Fig. 5b) shows that the coalesced bubble (4-region flow) regime occurs at 0.14 m s^{-1}, whereas the coalesced bubble (3-region flow) regime starts at 0.17 m s^{-1}. The first U_{trans} value obtained is 0.04 m s^{-1}, while the value predicted by the correlation of Reilly et al. [36] is 0.046 m s^{-1}. A comparison between Figs. 3b and 5b) shows that the KE values at P = 1.0 MPa are somewhat higher.

The U_{trans} results obtained from Figs. 3–5 are summarized in Tab. 1.

Table 1. Summary of various U_{trans} values identified in this work at P = 0.1, 0.4, and 1 MPa.

Hydrodynamic regime	U_{trans} [m/s]		U_{trans} [m/s]		U_{trans} [m/s]	
	P = 0.1 MPa		P = 0.4 MPa		P = 1.0 MPa	
	AAD	KE	AAD	KE	AAD	KE
First transition	0.02	0.02	0.03	0.03	0.04	0.04
Second transition	0.08	0.08	0.06	0.05	0.08	0.08
Coalesced bubble (4-region flow)	0.10	0.10	0.10	0.10	0.13	0.14
Coalesced bubble (3-region flow)	0.13	0.12	0.13	0.13	0.16	0.17

The transitional gas velocities, U_{trans}, obtained using deterministic chaos theory do not match with those estimated by means of the classical analyses such as the change in the slope of gas holdup curve and drift flux plot. In addition, the U_{trans} values obtained are in disagreement with those calculated using the break-point in steepness parameter of gas holdup radial profiles [10].

4 Conclusions

Flow regime identification is an important aspect in BC design and scale-up. It was shown that by means of both statistical (AAD) and chaotic (KE) parameters applied to CT data, one can successfully identify the boundaries of dispersed bubble, first transition, second transition, coalesced bubble (4-region flow), and coalesced bubble (3-region flow) regimes. The nonlinear chaos theory was applied for the first time to CT data. As the pressure increases, the first transition velocity shifts to higher u_G values. The third transition velocity appears to be

unaffected when pressure is changed from 0.1–0.4 MPa, whereas it increases when the pressure is changed to 1 MPa. The fourth transition velocity exhibits a similar trend to the third transition velocity.

It was found that the first transition velocity can always be reasonably predicted by the formulas of Reilly et al. [36]. At P = 0.4 MPa the second transition regime starts earlier. Basically, there is a good correspondence between the sudden changes (mostly minima) in the AAD values and the sudden changes (mostly maxima) in the KE values. The transitional gas velocities obtained by both statistical and chaotic parameters are quantitatively consistent. These values do not match with those obtained using classical methods such as the change in gas holdup curve and drift flux plot. However, it facilitates the differentiation of the multiple regimes that are present in bubble columns.

Acknowledgement

Dr. S. Nedeltchev expresses his gratitude to the Bulgarian-American "Fulbright" Commission for the research grant provided. The authors are also thankful to the High Pressure Slurry Bubble Column Reactor (HPSBCR) Consortium[ConocoPhillips (USA), EmiTech (Italy), Sasol (South Africa), Statoil (Norway)] and UCR-DOE (DE-FG-26-99FT40594) grants that made this work possible.

Symbols used

AAD	[bits]	average absolute deviation
D_c	[m]	column diameter
KE	[bits/s]	Kolmogorov entropy
L	[m]	aerated liquid height
N	[–]	number of data in a time series
P	[Pa]	operating pressure
Re_{0L}	[–]	orifice Reynolds number referred to the liquid phase (see [37])
u_G	[m/s]	superficial gas velocity
U_{trans}	[m/s]	transitional gas velocity
X	[–]	element in the time series

Greek Symbols

μ_L	[Pa s]	liquid viscosity
ρ_L	[kg m^{-3}]	liquid density
σ	[N m^{-1}]	liquid surface tension

Subscripts

i	number of the respective element in the time series
mean	mean value of the time series

References

[1] J. Zahradnik et al., *Chem. Eng. Sci.* **1997**, *52*, 3811.
[2] R. C. Chen, J. Reese, L.-S. Fan, *AIChE J.* **1994**, *40*, 1093.
[3] E. Olmos, C. Gentric, S. Poncin, N. Midoux, *Chem. Eng. Sci.* **2003**, *58*, 1731.
[4] E. Olmos, C. Gentric, N. Midoux, *Can. J. Chem. Eng.* **2003**, *81*, 382.
[5] S. Barghi, A. Prakash, A. Margaritis, M. A. Bergougnou, *Can. J. Chem. Eng.* **2004**, *82*, 865.
[6] C. Vial, S. Poncin, G. Wild, N. Midoux, *Chem. Eng. Proc.* **2001**, *40*, 135.
[7] T.-J. Lin, J. Reese, T. Hong, L.-S. Fan, *AIChE J.* **1996**, *42*, 301.
[8] S. Nedeltchev, U. Jordan, A. Schumpe, in *CD-ROM of the 7th Int. Conf. on Gas-Liquid and Gas-Liquid-Solid Reactor Engineering* (Ed: G. Wild), Strasbourg **2005**.
[9] S. Nedeltchev, U. Jordan, A. Schumpe, in *Prep. of the 7th German-Japanese Symposium on Bubble Columns* (Ed: A. Schumpe), Goslar, Germany **2006**.
[10] A. Shaikh, M. Al-Dahhan, *Flow Meas. Instrum.* **2005**, *16*, 91.
[11] D. Barnea, O. Shohan, Y. Taitel, *Int. J. Multiphase Flow* **1980**, *6*, 387.
[12] F. Franca, M. Acikgoz, R. T. Lahey Jr., A. Clausse, *Int. J. Multiphase Flow* **1991**, *17*, 545.
[13] R. K. Das, S. Pattanayak, *Meas. Sci. Tech.* **1993**, *4*, 1457.
[14] R. K. Das, S. Pattanayak, *Chem. Eng. Sci.* **1994**, *49*, 2163.
[15] J.-P. Zhang, J. R. Grace, N. Epstein, K. S. Lim, *Chem. Eng. Sci.* **1997**, *52*, 3979.
[16] H. M. Letzel, J. C. Schouten, R. Krishna, C. M. Van den Bleek, *Chem. Eng. Sci.* **1997**, *52*, 4447.
[17] T.-J. Lin, R.-C. Juang, Y.-C. Chen, C.-C. Chen, *Chem. Eng. Sci.* **2001**, *56*, 1057.
[18] T.-J. Lin, R.-C. Juang, C.-C. Chen, *Chem. Eng. Sci.* **2001**, *56*, 6241.
[19] V. V. Ranade, R. P. Utikar, *Chem. Eng. Sci.* **1999**, *54*, 5237.
[20] C. Vial et al., *Chem. Eng. Sci.* **2000**, *55*, 2957.
[21] R. Kikuchi et al., *Chem. Eng. Sci.* **1997**, *52*, 3741.
[22] M. Cassanello et al., *Chem. Eng. Sci.* **2001**, *56*, 6125.
[23] S. Nedeltchev, S. Kumar, M. P. Dudukovic, *Can. J. Chem. Eng.* **2003**, *81*, 367.
[24] C. M. Van den Bleek, J. C. Schouten, *Chem. Eng. J.* **1993**, *53*, 75.
[25] C. M. Van den Bleek, M.-O. Coppens, J. C. Schouten, *Chem. Eng. Sci.* **2002**, *57*, 4763.
[26] P. Grassberger, T. Schreiber, C. Schraffrath, *Int. J. Bifurcation Chaos* **1991**, *1*, 521.
[27] N. Rados, *D. Sc. Thesis*, Washington University, St. Louis, MO **2003**.
[28] N. Rados, A. Shaikh, M. H. Al-Dahhan, *Chem. Eng. Sci.* **2005**, *60*, 6067.
[29] S. B. Kumar, *D. Sc. Thesis*, Washington University, St. Louis, MO **1994**.
[30] S. B. Kumar, D. Moslemian, M. P. Dudukovic, *AIChE J.* **1997**, *43*, 1414.
[31] A. Kemoun et al., *Int. J. Multiphase Flow* **2001**, *27*, 929.
[32] B. Ong, *D. Sc. Thesis*, Washington University, St. Louis, MO **2003**.
[33] L.-S. Fan et al., *Chem. Eng. Sci.* **1999**, *54*, 4681.
[34] J. C. Schouten, F. Takens, C. M. Van den Bleek, *Phys. Rev. E* **1994**, *49*, 126.
[35] S. Nedeltchev, *Bulg. Chem. Ind.* **1998**, *69*, 35.
[36] I. G. Reilly, D. S. Scott, T. J. W. De Bruijn, D. MacIntyre, *Can. J. Chem. Eng.* **1994**, *72*, 3.
[37] D. Miller, *AIChE J.* **1974**, *20*, 445.

